Variable-Rate Adaptive Trellis Coded QAM for Flat-Fading Channels

Vincent K. N. Lau and Malcolm D. Macleod, *Member, IEEE*

***Abstract*—A bandwidth-efficient variable-rate adaptive channel coding scheme, ATCQAM, for time-varying flat-fading channels is proposed. In addition to the forward channel, a low-capacity feedback channel is needed to convey channel state information to the transmitter, possibly with delays and noise. A number of transmission modes, with varying throughputs, are incorporated at the transmitter. Appropriate transmission modes are selected based on the feedback channel states. Design issues for the ATCQAM are considered. A closed-loop control scheme to maintain mode synchronization between the transmitter and the receiver is discussed. The effects of feedback delay, a noisy feedback channel, and mobile speed are investigated. Analytical bounds are derived and simulations are performed to verify the results.**

***Index Terms*—Adaptive coded QAM, variable-rate adaptive channel coding.**

NOMENCLATURE

$c[r,k]$	Channel fading at the rth symbol of the kth user burst.
$z_{tx}[r,k]$	Estimated channel fading at the transmitter.
$z_{rx}[r,k]$	Estimated channel fading at the receiver.
$\epsilon_1[r]$	Residual noise of interpolation filtering at the receiver.
$\epsilon_2[r]$	Channel noise of the estimated fading at the receiver.
$\epsilon_3[r]$	Prediction noise of estimated fading at the transmitter.
$\epsilon_4[r]$	Channel noise of the estimated fading at the transmitter.
x_k	The kth modulation symbol transmitted.
y_k	The kth received symbol.
$\vec{s}$	Trellis state transition sequence.
$\vec{m}_N$	Mode sequence of length N.
$\bar{cta}$	Average throughput of the ATCQAM scheme.

I. INTRODUCTION

ERROR correction codes have been widely used to combat the effect of Rayleigh fading in mobile radio channels. In traditional FEC schemes [1], fixed-rate codes are used but they fail to exploit the time-varying nature of the channel. To keep the performance at a desirable level, they are designed for the average or worst-case situation. In this paper, we propose and study a bandwidth-efficient variable-rate adaptive trellis coded QAM (ATCQAM) which varies the code rate and modulation level according to the channel condition. The receiver estimates the channel states and informs the transmitter through the use of a feedback link. When the channel state is good, the transmitter increases the throughput by using a higher level QAM. On the other hand, when the channel state is bad, the transmitter uses a lower level QAM to improve the error protection at the expense of lower throughput.

The performance of uncoded adaptive transmission schemes for Rayleigh fading channels based on the feedback of channel state information has been considered in [2]. In [3], the fundamental reasons for performance gain for variable-rate adaptive systems has been investigated. Many practical variable-rate error correction codes have been proposed in recent years to reduce the bit error rate (BER) and to increase throughput of the mobile radio channels [4]–[6]. In particular, adaptive trellis coded modulation was considered in [4] which used a class of M-ary PSK symbols. However, these previous results were based on numerous simplifying assumptions such as coherent detection, perfect mode synchronization on the transmission modes, and zero feedback delay. In [7], a variable-power and variable-rate coded MQAM system based on coset codes was investigated based on perfect channel estimation and clean feedback with zero feedback delay. Issues of channel estimations and strong robustness were addressed recently in [8]. In [9], the effect of channel estimation noise is investigated based on static analysis of fixed-rate uncoded MQAM constellations. By contrast, this paper has the following important contributions. We unify the performance analysis of the adaptive system based on practical considerations of channel estimation noise, feedback noise, feedback delay, and mobile speed. Design issues such as mode synchronization and operational aspects are explicitly handled. In particular, closed-loop mode synchronization based on *skewed interleaving* is proposed to ensure that the receiver decodes the received symbols with appropriate modes. Two modes of operation of the ATCQAM scheme, namely *constant BER* operation and *constant average throughput* operation are introduced to utilize the adaptive system under different scenarios. Furthermore, traditional BER analysis for fixed-rate trellis codes, which is based on the conditional error probability of sequence of modulation symbols $(\vec{x})$ on trellis branches $P\left(\vec{x} \longrightarrow \vec{\hat{x}} | \vec{c}\right)$, could not be applied directly in adaptive systems in general. This is because the symbol sequence $\vec{x}$ itself depends on the modulation modes (and hence the channel state $\vec{c}$). A new BER analysis based on trellis state transition is proposed.

Paper approved for publication by N. C. Beaulieu, the Editor for Wireless Communications Theory of the IEEE Communications Society. Manuscript received September 29, 1997; revised April 20, 1999, September 23, 1999, February 11, 2000, and April 18, 2000. This paper was presented at the IEEE Vehicular Technology Conference '98, Ottawa, ON, Canada, September 1998.

V. K. N. Lau is with the Department of Electrical and Electronic Engineering, University of Hong Kong, Hong Kong (e-mail: knlau@eee.hku.hk).

M. D. Macleod is with the Engineering Department, Cambridge University, Cambridge CB2 IPZ, U.K. (e-mail: mdm@eng.cam.ac.uk).

Publisher Item Identifier S 0090-6778(01)08161-2.

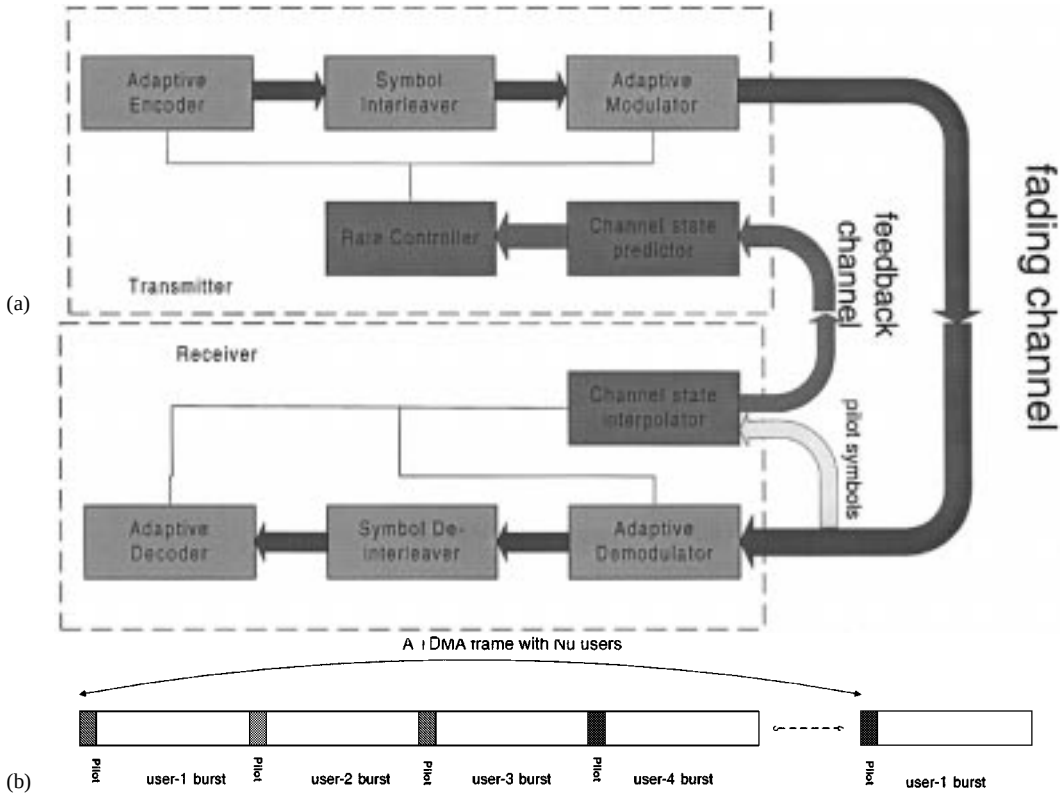

Fig. 1. Overall block diagram of ATCQAM scheme. (a) Transmitter and receiver of ATCQAM. (b) Frame structure.

The paper is organized as follows. In Section II, we describe the system model, design issues, system components, and the operation of the ATCQAM scheme. In Section III, analytical bounds for the ATCQAM system performance are formulated. Simulation and analytical results are presented and discussed in Section IV. Finally, in Section V, we conclude with a summary of results.

II. Proposed Adaptive Trellis Coded QAM System

The block diagram of the proposed scheme is shown in Fig. 1(a). At the transmitter, the system consists of a variable-rate convolutional encoder, a variable-throughput adaptive modulator, a symbol interleaver, and a channel state predictor. Information bits are convolutionally encoded and the coded bits are mapped onto the appropriate M-ary QAM symbol. The varying instantaneous throughput is achieved by encoding a varying number of information bits per symbol. Time division multiple access (TDMA) framing is assumed with N_u users per TDMA frame. Pilot symbols are transmitted periodically to aid channel state estimation at the receiver [10]. This is illustrated in Fig. 1(b).

At the receiver, we have the adaptive demodulator, a symbol de-interleaver, a single Viterbi decoder for all modes, and an interpolation filter. Channel states between the pilot positions are interpolated and used to demodulate the received symbols. The channel states at *pilot positions* are fed back to the transmitter via a noisy feedback link with certain delays. Using the linear prediction filter, current channel states are predicted at the transmitter and appropriate transmission modes are then selected for the current symbol.

A. Design of the Variable-Rate Channel Encoder

The design is based on the *pragmatic* TCM design [11] using a core rate $1/2$ encoder. Between each trellis transition, a variable number of uncoded bits are concatenated with the coded bits and mapped onto the appropriate M-ary QAM symbol as shown in Fig. 2(b). Hence, we have a trellis with a fixed number of states but a varying number of parallel branches between each transition step. Because the trellis structure remains the same for all different transmission modes, the same Viterbi decoder can be used at the receiver. Furthermore, all M-ary symbols have the same symbol duration and hence the occupied bandwidth is constant.

B. Operation of the ATCQAM

There are seven transmission modes in the proposed ATCQAM as illustrated in Table I.

The estimated channel state at the transmitter for the rth symbol at the kth burst, $z_{tx}[r,k]$, is partitioned into seven segments, with each segment corresponding to one of the modes in Table I. Let E_s/η_0 be the average symbol-energy-to-noise ratio. Mode m is chosen if $E_s/\eta_0|z_{tx}[r,k]|^2 \in [\zeta_m, \zeta_{m+1}]$. Note that $\zeta_0 = 0$ and $\zeta_7 = \infty$. There are two different ways to operate the ATCQAM scheme, namely *constant BER* operation and *constant average throughput* operation.

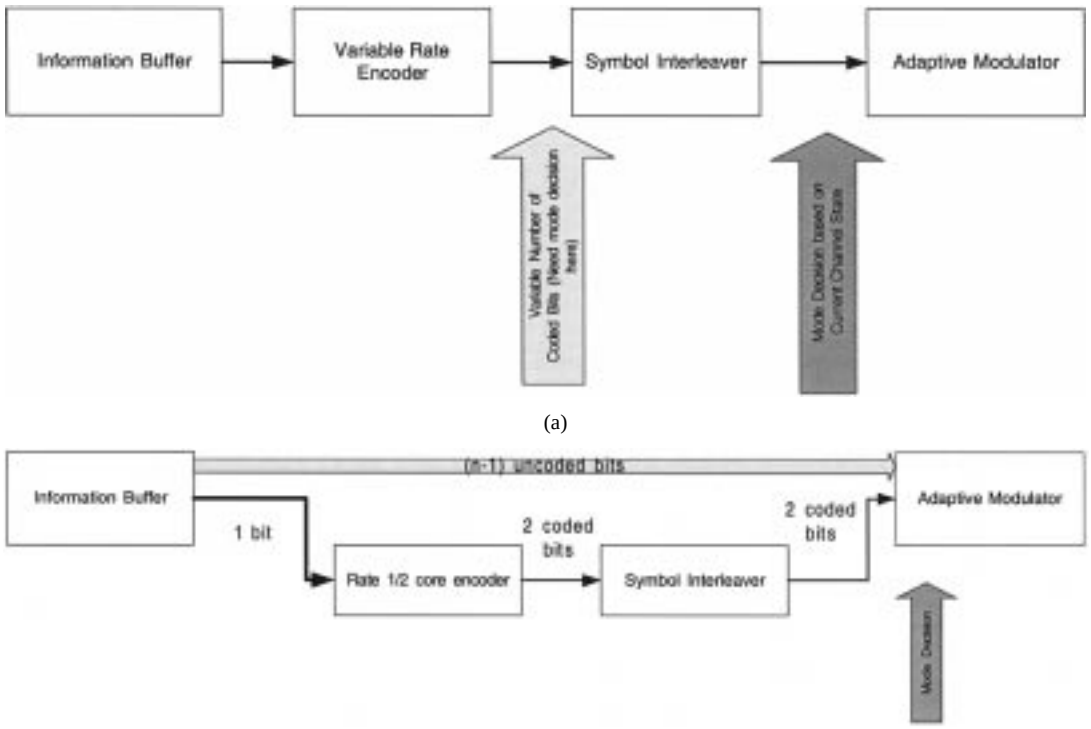

Fig. 2. Interleaving of the ATCQAM scheme. (a) Problems of traditional block interleaving. (b) Solution of interleaving in ATCQAM.

TABLE I
OPERATION MODES OF ATCQAM

Throughput	code mapping
1/3	6 coded bits mapped to 3 QPSK symbols
1/2	4 coded bits mapped to 2 QPSK symbols
1	2 coded bits mapped to 1 QPSK symbol
2	1 uncoded bit + 2 coded bits mapped to 1 8PSK symbol
3	2 uncoded bits + 2 coded bits mapped to 1 16QAM symbol
4	3 uncoded bits + 2 coded bits mapped to 1 32QAM symbol
5	4 uncoded bits + 2 coded bits mapped to 1 64QAM symbol

1) Constant BER Operation: For the constant BER operation, we set the switching thresholds[1] so as to maintain a relatively constant BER over a range of E_s/η_0. The set of thresholds is not a function of the average SNR. At high instantaneous SNR, we strive for a higher throughput instead of a lower BER. At low instantaneous SNR, we reduce the BER at the expense of a lower throughput. This mode of operation is ideal for variable-rate sources.

2) Constant Average Throughput Operation: Traditional fixed-rate codes are operating in a *constant throughput* operation in the sense that the average throughputs are the same for different BER values. However, for the ATCQAM scheme operating in *constant* BER, the average throughput along the BER curves is varying. Hence, it is not easy to compare the SNR gains between the fixed-rate codes and the ATCQAM scheme because the comparison of SNRs must be relative to the same throughput. For constant throughput operation of the ATCQAM scheme, we set the thresholds so as to maintain a constant average throughput[2] relative to different average SNR values. This constant average throughput control is useful when we connect a *fixed-rate source* to the ATCQAM system in a shadowing environment where the *local mean SNR* is variable.

C. Mode Synchronization

Mode synchronization is a very crucial requirement for the proper operation of the adaptive system because the receiver must decode the symbols with the correct mode. Mode synchronization can be attained with a closed-loop method. A control word describing the transmission modes for the burst is embedded into the burst-header as illustrated in Fig. 3(a). The control words for several bursts are grouped, protected with BCH codes, interleaved, and QPSK modulated. Note that control words are actually skewed up to the interleaving depth as shown in Fig. 3(b), and this is called *skewed interleaving.* At the receiver, the received signals are converted into two-dimensional symbols and stored up to the interleaving depth. The control words are deinterleaved and decoded first, followed by the rest of the burst which is decoded with the indicated transmission modes.

D. Feedback Channel

The feedback channel is used to carry fading channel state information. Since fading is a narrow-band random process with bandwidth given by the Doppler frequency,[3] f_d, the sampling rate of the fading process is $2f_d$ to avoid alaising. In most cases, this represents a very low-capacity requirement on the feedback

[1]Since a mode is chosen only when the instantaneous SNR is within a small range, the thresholds are obtained as follows. For each mode, the BER-SNR curves in an additive white Gaussian noise (AWGN) channel are plotted. Suppose we want to operate at a BER level of 10^{-3}. A horizontal line corresponding to the specified BER level is drawn and the SNR thresholds for different modes are obtained from the intersections of the line and the BER curves.

[2]This can be achieved if the set of thresholds are scaled by the average SNR E_s/η_0 (see Section III-E).

[3]In this paper, we assume $f_d \approx 90$ Hz for a mobile speed of 50 km/h and a baud rate (per user) of 40 k symbols/s.

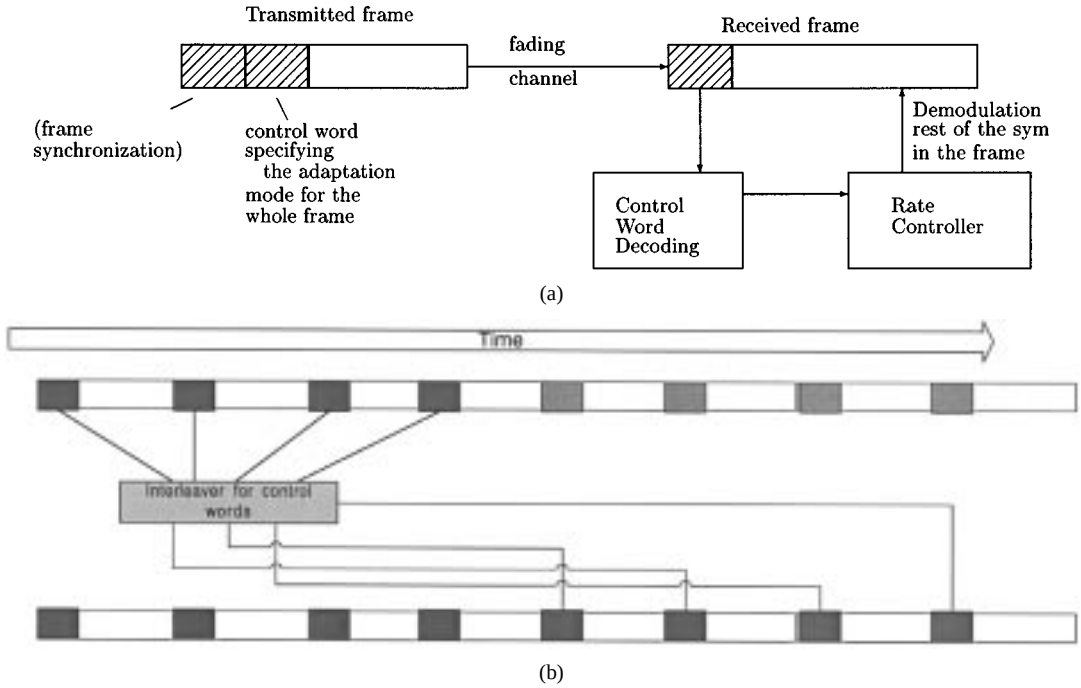

Fig. 3. Issues on mode synchronization. (a) Closed-loop mode synchronization. (b) Interleaving of control words.

channel. In this paper, fading samples are quantized with 8-bit μ-law.[4] The five most significant bits of each quantized sample is further protected with a BCH(15,5) code. The total of 18 bits are then QPSK modulated. The total baud rate on the feedback channel is around 1620 symbols per second. This is very low compare with the forward baud rate of 40 k symbols per second. The effect of noisy feedback is investigated by simulations with the SNR as a parameter (see Section IV).

E. Interleaving

Interleaving is used to convert the bursty fading into independent fading. Conventionally, a block interleaver is inserted after the channel encoder and before the modulator. For traditional fixed-rate systems, the interleaving task (symbol interleaving—a symbol is comprised of several coded bits) is straightforward because the number of coded bits entering the interleaver is always fixed. However, in general adaptive systems, the interleaving task is not trival. The throughput per symbo, and the number of *coded bits* carried by modulation symbols (per trellis transition) are variable depending on modes. This implies that a variable number of coded bits should enter the block interleaver as illustrated in Fig. 2(a). To determine the appropriate number of bits to enter the interleaver, it is necessary to determine the transmission mode for that symbol beforehand. However, the transmission mode is solely determined by the channel state at the moment when that symbol is taken out of the interleaver and actually transmitted. There is a huge delay from the time the symbol enters the interleaver and the time the symbol leaves the interleaver. Hence, we have a deadlock problem and special arrangement of interleaving is necessary.

In this ATCQAM, we take advantage of the pragmatic code design. Output bits from the pragmatic encoder are separated into a coded stream and an uncoded stream as illustrated in Fig. 2(b). The coded stream is produced by a fixed-rate core encoder (1/2) and hence the number of bits out of the coded stream per trellis transition is always fixed. The coded stream is interleaved by conventional methods. The uncoded stream is not interleaved and variable throughput is eventually achieved by taking a different number of *uncoded bits* to make up a modulation symbol. In this way, the mode decision process could be *deferred* to the modulation stage without affecting the interleaving process.

F. Channel State Estimation at the Receiver

Pilot symbols are transmitted (one pilot every N_p symbols) to aid channel estimation at the receiver. The receiver stores a number of pilot symbols and makes use of an *interpolation filter* to estimate the fading between pilot symbols. Assume the Doppler spread of the fading process is f_d. By the Nyquist sampling theorem, perfect reconstruction is possible if

$$f_d N_p T_s < 0.5. \tag{1}$$

Firstly, a symbol is labeled by the coordinate (r, i), indicating the rth symbol at the ith burst. Hence, let $c[r, i]$ be the complex fading at symbol (r, i). It could be shown in [12] that the estimated channel state at the symbol position (r, i), $z_{rx}[r, i]$, using a $(2P_1 + 1)$th-order finite-impulse response (FIR) interpolation filter is given by

$$\begin{aligned} z_{rx}[r,i] &= \sum_{p=-P_1}^{P_1} h_{p,r} z_{rx}[0,p] \\ &= \overbrace{\left[\sum_{p=-P_1}^{P_1} h_{p,r} c[0,p]\right]}^{c[r,i]+\epsilon_1[r,i]} + \overbrace{\left[\sum_{p=-P_1}^{P_1} h_{p,r} \tilde{e}[p]\right]}^{\epsilon_2[r,i]}, \\ r &\in [1, N_p - 1] \end{aligned} \tag{2}$$

[4] μ-law is a PCM companding standard used in the American T-carrier digital hierarchy

where $h_{p,r}=\mathrm{sinc}(\mathrm{i}+\mathrm{r}/(\mathrm{N_p}\mathrm{N_u}))$, N_u is the number of users per TDMA frame, and $z_{rx}[0,p]$is the fading estimate at pilot position $(0,p)$. Note that $\epsilon_1[r,i]$ and $\epsilon_2[r,i]$ are Gaussian[5] random variables. The variance of $\epsilon_2[r,i]$ is given by

$$\sigma_2^2[r]\stackrel{\mathrm{def}}{=}\mathcal{E}[|\epsilon_2[r,i]|^2]=\sigma_{\tilde{e}}^2\sum_{p=-P_1}^{P_1}h_{p,r}^2. \tag{3}$$

Hence, the interpolated fading estimate at the receiver $z_{rx}[r,i]$ is modeled as a correct fading $c[r,i]$, corrupted with channel noise $\epsilon_2[r,i]$ and the residual noise $\epsilon_1[r,i]$. The receiver uses $z_{rx}[r,i]$ to perform matched filtering and to compute the decision metrics to be used in the Viterbi decoder.

G. Channel State Estimation at the Transmitter

To reduce the required feedback capacity, only the estimated channel states (at the receiver) at pilot positions $z_{rx}[0,i]$ are fed back to the transmitter with a delay of Δ. The current channel state is estimated at the transmitter based on the feedback pilot estimates $z_{rx}[0,i]$ using *linear predictive filtering* [13]. It is shown in [12] that the P_2-order predicted fading for symbol (r,k), $z_{tx}[r,k]$ is given by

$$z_{tx}[r,k]=\begin{cases}z_{tx}[0,k]=c[0,k]+\epsilon_3[0,k]+\epsilon_4[0,k], & r\in[0,\Delta)\\ z_{rx}[0,k]=c[0,k]+\tilde{e}[0,k], & r\in[\Delta,N_p]\end{cases} \tag{4}$$

where

N_p	pilot symbol period;
$\epsilon_3[0,k]$	prediction noise (which is Gaussian at large P_2);
$\epsilon_4[0,k]$	channel noise.

III. Performance Analysis

In this section, we derive analytical bounds on the ATCQAM performance. A path, labeled by (i), in the trellis diagram is defined as a sequence of trellis state transitions, $\vec{s}_N(i)=\{s_0(i),s_1(i),\ldots,s_N(i)\}$. The nth trellis state $s_n(i)$ is a function of $s_{n-1}(i)$ and $u_n(0)$ only where $u_n(0)$ is the least significant input bit at the nth trellis transition. Hence, the state sequence (or state path) is independent of the transmission mode. On the other hand, the nth encoded symbol x_n is a function of $s_{n-1}(i)$, $s_n(i)$, $|z_{tx}[n]|$, and $u_n(0),u_n(1),\ldots$. Thus, the encoded symbol sequence $\vec{x}$ is dependent on the transmission modes. Because of this, conventional analysis methods for fixed-rate TCMs which analyze the BER based on the encoded symbol sequence is not applicable here. We shall analyze the BER of the ATCQAM based on the state sequence. The effect of feedback delay is included in the derivations. Similar to [4], [7], ideal interleaving is assumed to simplify the analysis.

[5]$\epsilon_1[r,i]$ is the *residual* noise due to imperfect interpolation and is modeled as Gaussian. $\epsilon_2[r,i]$ is a sum of $2P_1+1$ uncorrelated Gaussian variables and hence is Gaussian distributed.

A. Equivalent Channel Model and Decision Metric

Fading for all encoded symbols on the error path is assumed to be independent. The kth received symbol corresponding to the rth symbol position[6] $y_k(r)$ is given by

$$y_k(r)=\sqrt{2E_s}c[r,k]x_k+n_k \tag{5}$$

where $c[r,k]$ is an independent complex Gaussian fading process for the symbol (r,k) with variance $\mathcal{E}[|c[r,k]|^2]=1$, x_k is the transmitted symbol normalized to unit variance $(\mathcal{E}[|x_k|^2]=1)$, and n_k is a complex white Gaussian channel noise with $\mathcal{E}[|n_k|^2]=2\eta_0$. For simplicity, we drop the subscript k in $c[r,k]$, $z_{rx}[r,k]$, and $z_{tx}[r,k]$ when there is no ambiguity.

Since the receiver only has knowledge of the estimated fading $z_{rx}[r]$, we substitute (2) into (5), express $y_k(r)$ in terms of $z_{rx}[r]$, E_s, and normalize w.r.t. $2\eta_0$, giving

$$y_k'(r)=\sqrt{\frac{E_s}{\eta_0}}z_{rx}[r]x_k+n_k' \tag{6}$$

where $n_k'=n_k/2\eta_0-\sqrt{E_s/\eta_0}x_k(\epsilon_1[r]+\epsilon_2[r])$ is a Gaussian noise. Its variance (depending on r) is given by

$$\begin{aligned}\mathcal{E}[|n_k'|^2]=&\sigma_{n'}^2(r)\\ =&1+\sqrt{\frac{E_s}{\eta_0}}|x_k|^2\left(\sigma_1^2[r]+\sigma_2^2[r]\right)\\ \le&1+\sqrt{\frac{E_s}{\eta_0}}|b|^2\left(\sigma_1^2[r]+\sigma_2^2[r]\right)\end{aligned} \tag{7}$$

where $|b|=\max|x_k|$. The maximum likelihood branch decision metric, $\mu_{ML}(x_k,r)$, is given by

$$\begin{aligned}\mu_{ML}(x_k,r)=&p(y_k(r)|x_kz_{rx}[r])\\ =&\frac{|y_k(r)-\sqrt{\frac{E_s}{\eta_0}}z_{rx}[r]x_k|^2}{\sigma_{n'}^2(r)}\end{aligned}$$

and we choose x_k so that $\mu_{ML}(x_k,r)$ is minimum.

B. Error Probability

Bit errors are due to either path errors or parallel branch errors. The average BER, $\bar{P}_b$, is given by

$$\bar{P}_b=\bar{P}_b(\vec{s}(i)\longrightarrow\vec{s}(j))+\bar{P}_{||} \tag{8}$$

where $\vec{s}(j)$ is the estimated state sequence and $\vec{s}(i)$ is the actual transmitted state sequence. The above two terms, $\bar{P}_b(\vec{s}(i)\longrightarrow\vec{s}(j))$ and $\bar{P}_{||}$, are derived as follows.

C. Upper Bound on $\bar{P}_b(\vec{s}(i)\longrightarrow\vec{s}(j))$

Consider the case when $\vec{s}_N(j)$ diverges from $\vec{s}_N(i)$ at node-0 and remerges at node-N. Let $\vec{m}_N=\{m_1,m_2,\ldots,m_N\}$ be the sequence of transmission modes, with $m_n\in[0,6]$. Let $\mathcal{X}_i(\vec{m}_N)$ be the set that contains all encoded symbol sequences resulting

[6]We assume that all encoded symbols on the length-N error path belong to the same burst-position r from different bursts after de-interleaving.

from the same path, $\vec{s}_N(i)$, under the transmission mode sequence, $\vec{m}_N$. The average BER is given by [14]

$$\bar{P}_b\left(\vec{s}(i) \longrightarrow \vec{s}(j)\right) \le \frac{\mathcal{E}[n_b]}{\bar{n}} \tag{9}$$

where $\mathcal{E}[n_b]$ is the average number of bit errors per trellis transition and $\bar{n}$ is the average number of information bits transmitted per trellis transition. It is shown in Appendix A that $\mathcal{E}[n_b]$ is given by

$$\begin{aligned}\mathcal{E}[n_b] \le & \sum_{N=N_{\min}}^{\infty} \sum_{i} P(\vec{s}_i) \\ & \times \sum_{j \ne i} \sum_{\vec{m}_N} \sum_{\vec{x} \in \mathcal{X}_i(\vec{m}_N)} P(\vec{x}_N, \vec{m}_N | \vec{s}_i) \\ & \times \sum_{\hat{\vec{x}} \in \mathcal{X}_j(\vec{m}_N)} \beta\left(\vec{x}_N, \hat{\vec{x}}_N\right) \bar{P}\left(\vec{x}_N \longrightarrow \hat{\vec{x}}_N, \vec{m}_N\right)\end{aligned}$$

where $\beta\left(\vec{x}_N, \hat{\vec{x}}_N\right)$ is the number of bit errors associated with the error event $\vec{x}_N \longrightarrow \hat{\vec{x}}_N$, $N_{\min}$ is the constraint length of the code, and N_p is the burst length. Furthermore, $\bar{P}\left(\vec{x}_N \longrightarrow \hat{\vec{x}}_N, \vec{m}_N\right)$ is derived in Appendix A.

On the other hand, the average number of transmitted information bits $(\bar{n})$ is derived in Appendix B and is given by

$$\begin{aligned}\bar{n} = & \frac{1}{N_p - 1} \sum_{r=1}^{N_p - 1} \left[1 + \frac{1}{6} \exp\left\{-\frac{\zeta_2}{2\sigma_b^2(r)\frac{E_s}{\eta_0}}\right\}\right. \\ & + \frac{1}{2} \exp\left\{-\frac{\zeta_3}{2\sigma_b^2(r)\frac{E_s}{\eta_0}}\right\} \\ & + \exp\left\{-\frac{\zeta_4}{2\sigma_b^2(r)\frac{E_s}{\eta_0}}\right\} \\ & \left. + \cdots + \exp - \frac{\zeta_6}{2\sigma_b^2(r)\frac{E_s}{\eta_0}}\right].\end{aligned}$$

D. Upper Bound on $\bar{P}_{\|}$

Due to parallel branches, errors can still occur even when $\vec{s}(i) = \vec{s}(j)$. $\bar{P}_{\|}$ is given by

$$\begin{aligned}\bar{P}_{\|} = & \frac{1}{N_p - 1} \sum_{r=1}^{N_p - 1} \sum_{m=3}^{6} \int_{\zeta_m/(E_s/\eta_0)}^{\zeta_{m+1}/(E_s/\eta_0)} \\ & \int_0^{\infty} \left(P_{\|}(m,r) f(|z_{rx}| \,|\, |z_{tx}|) d|z_{rx}|\right) f(|z_{tx}|) d|z_{tx}|\end{aligned} \tag{10}$$

where $P_{\|}(m,r)$ is given by

$$P_{\|}(m,r) \le \frac{1}{2\lambda_m} \exp\left\{-\frac{E_s}{4\eta_0(1+\delta_r)} |z_{rx}|^2 |\Delta x_m|^2\right\} \tag{11}$$

and $f(.)$ is the probability density function derived in Appendix A. Note that λ_m is the number of bits transmitted per trellis transition at mode m. $|\Delta x_m|^2$ is the minimun Euclidean distance between the parallel branches at mode m.

E. Average Throughput

Due to the adaptive nature of ATCQAM, the number of bits carried per modulation symbol varies according to $|z_{tx}|$. The average normalized throughput $\bar{\eta}$, expressed as the average number of information bits carried per symbol duration (T_s), is given by

$$\begin{aligned}\bar{\eta} = & \frac{1}{N_p - 1} \sum_{r=1}^{N_p - 1} \\ & \cdot \left[\frac{1}{3}\Pr\left(0 \le z_{tx} < \zeta_1\right) + \cdots + 5\Pr\left(\zeta_6 \le Z_{tx} < \infty\right)\right]\end{aligned} \tag{12}$$

which can be simplified to

$$\begin{aligned}\bar{\eta} = & \frac{1}{N_p - 1} \sum_{r=1}^{N_p - 1} \left[\frac{1}{3} \int_{\sqrt{\zeta_0/(E_s/\eta_0)}}^{\sqrt{\zeta_1/(E_s/\eta_0)}} f(|z_{tx}|) d|z_{tx}| + \cdots \right. \\ & \left. + 5 \int_{\sqrt{\zeta_6/(E_s/\eta_0)}}^{\infty} f(|z_{tx}|) d|z_{tx}|\right] \\ = & \frac{1}{N_p - 1} \sum_{r=1}^{N_p - 1} \left[\frac{1}{3} + \frac{1}{6} \exp\left\{-\frac{\zeta_1}{2\sigma_b^2(r)\frac{E_s}{\eta_0}}\right\}\right. \\ & + \frac{1}{2} \exp\left\{-\frac{\zeta_2}{2\sigma_b^2(r)\frac{E_s}{\eta_0}}\right\} \\ & + \exp\left\{-\frac{\zeta_3}{2\sigma_b^2(r)\frac{E_s}{\eta_0}}\right\} \\ & \left. + \cdots + \exp\left\{-\frac{\zeta_6}{2\sigma_b^2(r)\frac{E_s}{\eta_0}}\right\}\right].\end{aligned} \tag{13}$$

F. Irreducible Error Floor

From (2), the estimated channel state at the receiver $(z_{rx}[r,i])$ is corrupted by the channel noise $\epsilon_2[r,i]$ and the residual error $\epsilon_1[r,i]$. Under normal conditions,[7] $\sigma_1^2[r]$ is negligible. However, at high fading rates, imperfect interpolation filtering results in significant $\sigma_1^2[r]$.

Assume that $E_s/\eta_0 \to \infty$. Then, from (3), $\sigma_1^2[r] \to 0$ and we have from (18)

$$\frac{E_s}{2\eta_0(1+\delta_r)} = \frac{1}{\frac{2\eta_0}{E_s} + \sigma_1^2[r] + \sigma_2^2[r]} \to \frac{1}{\sigma_2^2[r]}. \tag{14}$$

Hence, we have an irreducible error floor (determined by $\sigma_2^2[r]$) which cannot be reduced by increasing E_s/η_0.

IV. Results and Discussion

Due to the varying throughput in the ATCQAM scheme, we use the average symbol-energy-to-noise ratio E_s/η_0 instead of the usual bit-energy-to-noise ratio as a reference for comparison. We assumed $N_p = 91$ (pilot period), $P_1 = 21$ (interpolation filter order), $P_2 = 16$ (prediction filter order), and $N_u = 8$ (user per TDMA frame). The overhead due to pilot symbols is about 1%. A convolutional code of constraint length 5 is used to construct the ATCQAM. Its performance is compared with that of the fixed-rate TCM.

A. Performance of ATCQAM

1) Zero Feedback Delay $(\Delta = 0)$*:* As an illustration, we assumed zero feedback delay, a noiseless feedback channel,

[7]Normal conditions here mean that the Nyquist sampling criterion (1) is satisfied.

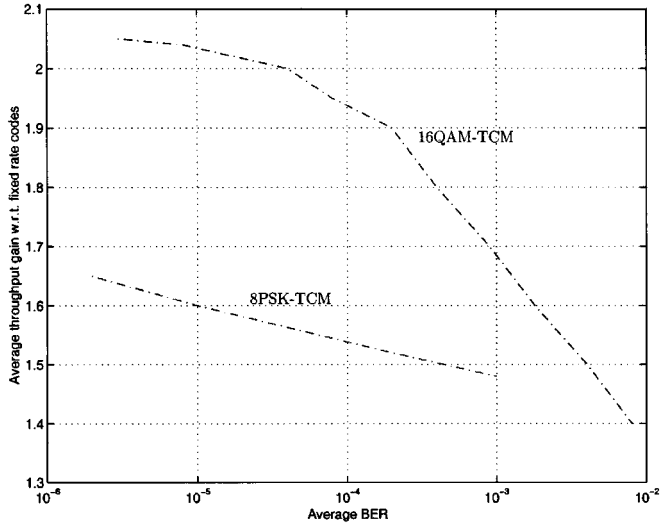

(a)

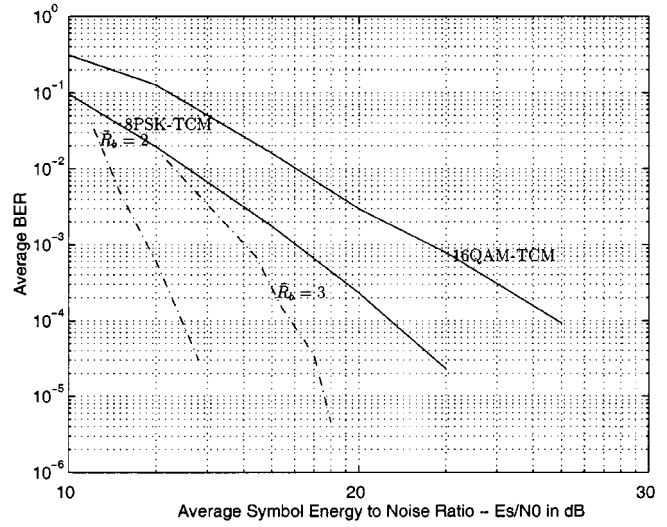

(b)

Fig. 4. Performance of ATCQAM relative to (a) 8PSK-TCM and (b) 16QAM-TCM. Dotted lines represent ATCQAM. Solid lines represent fixed rate codes.

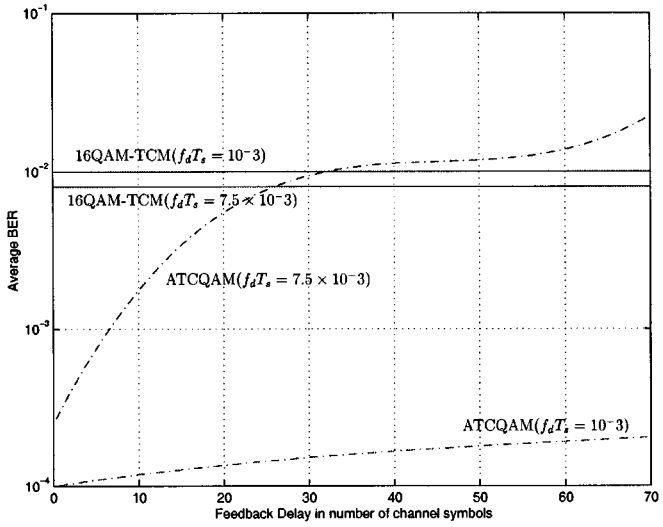

(a)

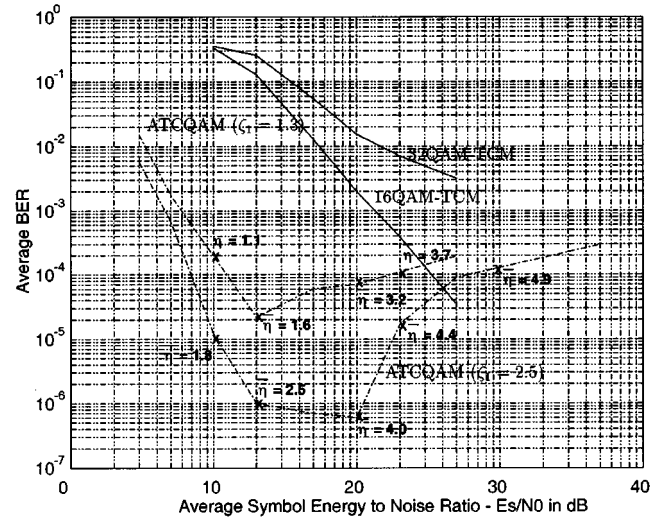

(b)

Fig. 5. Effects of (a) feedback delay and (b) mobile speed.

100×500 block interleaving[8] and $f_dT_s = 1 \times 10^{-3}$. When operating in *constant BER* mode, the relative throughput gains of ATCQAM relative to the fixed-rate 8PSK-TCM and 16QAM-TCM are plotted in Fig. 4(a). For example, if we control the BER at $\bar{P}_b = 10^{-4}$, the throughput gains relative to the 8PSK-TCM and the 16QAM are 1.95 and 1.54 times, respectively. On the other hand, when operating in *constant throughput* mode, the throughput of the ATCQAM is maintained at 2 and 3 bits per symbol (irrespective of E_s/η_0) for comparison with fixed-rate 8PSK-TCM and 16QAM-TCM, respectively. The E_s/η_0 gain of ATCQAM relative to 8PSK-TCM and 16QAM-TCM is plotted in Fig. 4(b). For example, there are 7.1-dB and 9.3-dB gains in E_s/η_0 at $\bar{P}_b = 10^{-4}$ relative to 8PSK-TCM and 16QAM-TCM, respectively.

2) Effects of Feedback Delay: The $\bar{P}_b$ of ATCQAM with finite feedback delay at $f_dT_s = 1 \times 10^{-3}$ and $f_dT_s = 7.5 \times 10^{-3}$ are shown in Fig. 5(a) with SNR $E_s/\eta_0 = 60$ dB and throughput $\bar{\eta} = 3$. The ATCQAM scheme is robust to the feedback delay in slow fading [see Fig. 5(a)]. For example, at a delay of $\Delta = 40$ symbols, $\bar{P}_b$ of the ATCQAM schemes is approximately 30 times smaller than the BER of fixed-rate 16QAM. At higher fading rates, it becomes more sensitive to the feedback delay. At $\Delta = 40$, $\bar{P}_b$ for ATCQAM degrades to that of fixed-rate 16QAM.

3) Effects of Mobile Speed: Fig. 5(b) shows $\bar{P}_b$ against E_s/η_0 for the ATCQAM scheme and for fixed-rate 16QAM-TCM at $f_dT_s = 7.5 \times 10^{-3}$. This figure illustrates the performance of the ATCQAM scheme at extreme mobile speeds where the sampling rate of the fading process is below the Nyquist rate. Hence, aliasing occurs in the channel estimation. The scheme operates at a *constant BER* control and, hence, the average throughput along the BER curves varies as illustrated. It is observed that the BER decreases at first but increases to an *irreducible* error floor at $\bar{P}_b = 3 \times 10^{-4}$ as the SNR increases. There are two reasons for this behavior.

[8]This corresponds to a mobile speed of 24 km/hr with baud rate (per user) of 40 k baud.

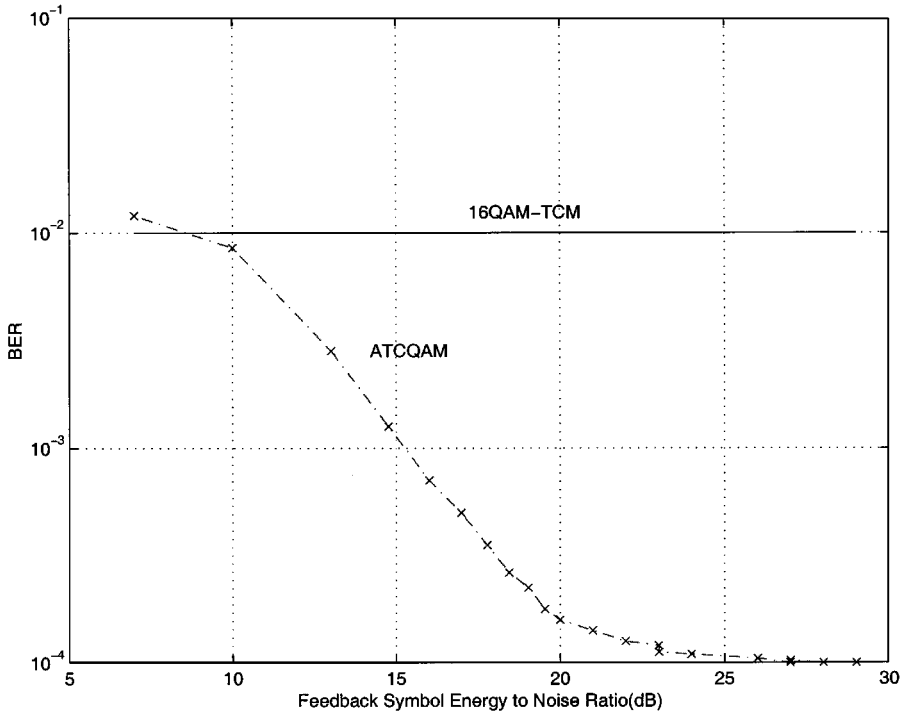

Fig. 6. Effect of noisy feedback $E_s/\eta_0 = 60$ for the forward channel. $\bar{\eta} = 3$, $f_d T_s = 1 \times 10^{-3}$.

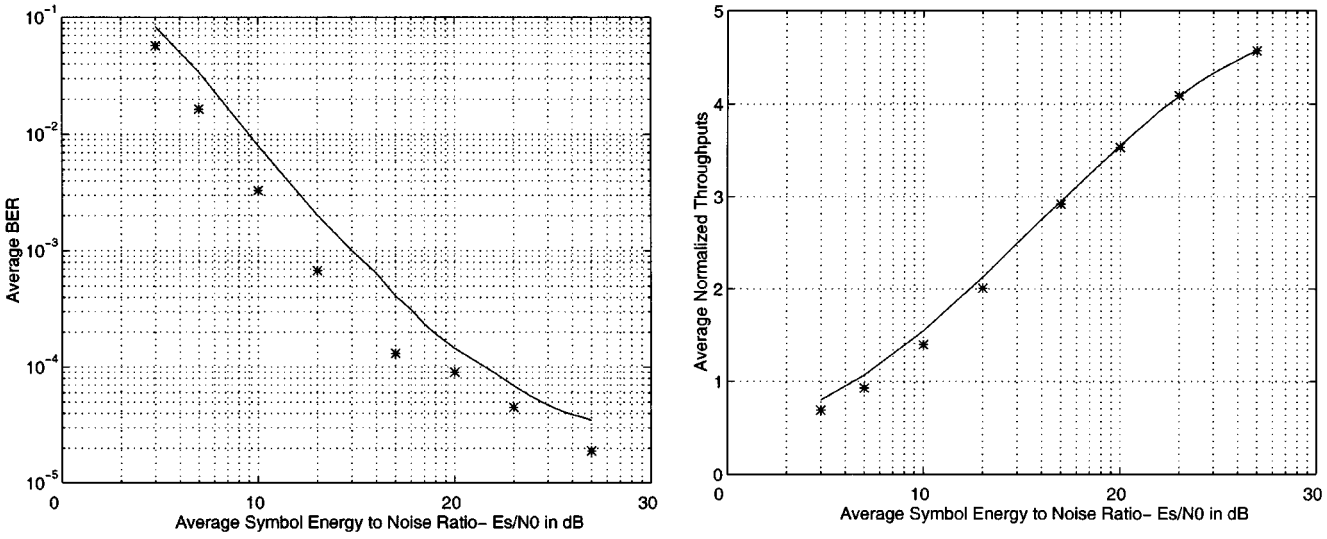

(a) (b)

Fig. 7. Comparision of analytical bounds (solid line) with the simulation results (*) of ATCQAM at feedback delay, $\Delta = 20$. (a) BER versus E_s/η_0. (b) Throughput versus E_s/η_0.

Firstly, aliasing causes residual noise ($\epsilon_2[r]$) in the channel estimation at the receiver. The adverse effect of residual noise is particularly serious for high-density constellations like 32QAM and 64QAM. Secondly, this behavior is due to fact that the adapatation thresholds are not designed for this extreme mobile speed.[9] Hence, the ATCQAM is forced to switch to a high throughput mode which is inappropriate due to the high residual noise.

4) Effects of Noisy Feedback: Fig. 6 shows the performance degradations due to a noisy feedback link. Robustness of the ATCQAM is studied with the average feedback SNR (E_{fb}/η_0) as a parameter where E_{fb} is the transmitted QPSK symbol energy in the feedback channel. It is found that the scheme is relatively robust. For example, at $E_{fb}/\eta_0 = 15$ dB, the BER of the ATCQAM is around 10 times lower than that of fixed-rate 16QAM-TCM. Actually, the effect of noisy feedback is similar to a delayed feedback in the sense that we have an inaccurate channel state for mode decision. However, the robustness could be explained by the fact that predicted channel states are not involved with demodulation or detection directly. The mode decision intervals are usually wide enough to accomodate reasonable prediction error of channel states.

[9]Thresholds are set without taking into account the residual noise.

B. Analytical Bounds for ATCQAM

The upper bounds on the BER ($\bar{P}_b$) and the average throughput ($\bar{\eta}$) of the ATCQAM scheme are evaluated using expressions in Section III at feedback delay ($\Delta = 20$) and are shown in Fig. 7(a) and (b). The BER bound is reasonably tight and follows the general trends of the BER curve. The throughput curve is accurate in that it matches nicely with the analytical model described in Section III.

It is mentioned in Section II that parallel branches are not detrimental to the performance of ATCQAM. This can be seen from (27) in Appendix A and (11). For a fixed-rate code with parallel branches, the BER in a Rayleigh fading channel will be dominated by $\bar{P}_{\|}$ (fixed). The dependency of E_s/η_0 in $\bar{P}_{\|}$ (fixed) is given by the factor $1/(E_s/\eta_0)$[15]. This gives rise to the undesirable single diversity order performance. Hence, in the fixed-rate code design, parallel branches have to be avoided.

On the other hand, when ATCQAM is operated under the *constant throughput* control, $\zeta_m \propto E_s/\eta_0$. Hence, there still remains an exponential dependency of E_s/η_0 in the expression of $\bar{P}_{\|}$(11) after integration in addition to the usual $1/(E_s/\eta_0)$ factor. By careful design of the signal constellation, the effect of parallel branches can be reduced. Due to the exponential dependency of E_s/η_0 in (27), a high effective diversity order BER performance [see Fig. 4(b)] is observed for the ATCQAM.

V. Conclusion

An ATCQAM scheme with seven transmission modes is proposed to exploit the time-varying nature of the mobile radio channel. To enable coherent demodulation of QAM symbols, pilot symbols are transmitted periodically. Estimated channel states at pilot positions are fed back to the transmitter via a feedback link. Design issues of the ATCQAM are briefly described and *constant BER* and *constant average throughput* operations are introduced for the variable-rate source and constant-rate source, respectively. A *closed-loop* control scheme is used to maintain mode synchronization between the transmitter and the receiver. Under normal operating conditions, ATCQAM has relative throughput gains around 1.5–1.9 times and relative E_s/η_0 gains around 8–9 dB relative to fixed-rate codes at $\bar{P}_b = 10^{-4}$. The effects of feedback link delay, noisy feedback, mobile speed, and issues of transmitter–receiver mode synchronization are considered. It is found that the ATCQAM scheme is robust in most practical situations. At $f_dT_s = 7.5 \times 10^{-3}$, an irreducible error floor occurs due to alaising of fading samples, causing channel state estimation errors.

Appendix A
Derivation of $\mathcal{E}[n_b]$

The node error probability corresponding to an error path of length N at burst position r, $P_e(N|\vec{m}_N, r)$, with the mode sequence $\vec{m}_N$ is given by

$$\begin{aligned} P_e(N|\vec{m}_N, r) &= \sum_i P(\vec{s}_N(i))\Pr\left[\bigcup_{j\neq i}(\vec{s}_N(i) \longrightarrow \vec{s}_N(j))|r\right] \\ &\leq \sum_i P(\vec{s}_N(i)) \sum_{j\neq i} P(\vec{s}_N(i) \longrightarrow \vec{s}_N(j)) \\ &= \sum_i P(\vec{s}_N(i)) \\ &\quad \times \sum_{j\neq i} \sum_{\vec{x}_N \in \mathcal{X}_i(\vec{m}_N)} P(\vec{x}_N|\vec{s}_N(i), \vec{m}_N) \\ &\quad \times \Pr\left[\bigcup_{\vec{\hat{x}}\in\mathcal{X}_j(\vec{m}_N)} \left(\vec{x}_N \longrightarrow \vec{\hat{x}}_N|\vec{m}_N, r\right)\right] \\ &\leq \sum_i P(\vec{s}_N(i)) \\ &\quad \times \sum_{j\neq i} \sum_{\vec{x}_N \in \mathcal{X}_i(\vec{m}_N)} P\left(\vec{x}_N|\vec{s}_N(i), \vec{m}_N\right) \\ &\quad \times \sum_{\vec{\hat{x}}\in\mathcal{X}_j(\vec{m}_N)} P\left(\vec{x}_N \longrightarrow \vec{\hat{x}}_N|\vec{m}_N, r\right). \end{aligned} \tag{15}$$

Hence, the unconditional node error probability is given by

$$P_e(N) = \frac{1}{N_p - 1} \sum_{r=1}^{N_p-1} \sum_{\vec{m}_N} P_e(N|\vec{m}_N, r)$$

and the *expected* number of bit errors per trellis transition, $\mathcal{E}[n_b]$, is given by[10]

$$\begin{aligned} \mathcal{E}[n_b] \leq & \sum_{N=N_{\min}}^{\infty} \sum_i P(\vec{s}_i) \\ & \times \sum_{j\neq i} \sum_{\vec{m}_N} \sum_{\vec{x}\in\mathcal{X}_i(\vec{m}_N)} P(\vec{x}_N, \vec{m}_N|\vec{s}_i) \\ & \times \sum_{\vec{\hat{x}}\in\mathcal{X}_j(\vec{m}_N)} \beta\left(\vec{x}_N, \vec{\hat{x}}_N\right) \bar{P}\left(\vec{x}_N \longrightarrow \vec{\hat{x}}_N, \vec{m}_N\right) \end{aligned} \tag{16}$$

where

$$\begin{aligned} &\bar{P}\left(\vec{x}_N \longrightarrow \vec{\hat{x}}_N, \vec{m}_N\right) \\ &\quad = \frac{1}{N_p - 1} \sum_{r=1}^{N_p-1} P\left(\vec{x}_N \longrightarrow \vec{\hat{x}}_N, \vec{m}_N|r\right) \end{aligned} \tag{17}$$

[10]Note that fixed-rate code is a special case of ATCQAM with only one mode. With a single mode, $\mathcal{X}_i(\vec{m}_N)$ becomes the set containing all encoded symbol sequences associated with path $\vec{s}_N(i)$. Hence,

$$\begin{aligned} \mathcal{E}[n_b] &\leq \sum_{N=N_{\min}}^{\infty} \sum_i P(\vec{s}_N(i)) \\ &\quad \times \sum_{i\neq j} \sum_{\vec{m}_N} \sum_{\vec{x}_N\in\mathcal{X}_i(\vec{m}_N)} P(\vec{x}_N, \vec{m}_N \mid \vec{s}_N(i)) \\ &\quad \times \sum_{\vec{\hat{x}}_N\in\mathcal{X}_j(\vec{m}_N)} \beta\left(\vec{x}_N, \vec{\hat{x}}_N\right) \bar{P}\left[\vec{x}_N \longrightarrow \vec{\hat{x}}_N, \vec{m}_N\right] \\ &\leq \sum_{N=N_{\min}}^{\infty} \sum_i \sum_{\vec{x}_N\in\mathcal{X}_i} P(\vec{s}_N(i), \vec{x}_N) \\ &\quad \times \sum_{j\neq i} \sum_{\vec{\hat{x}}_N\in\mathcal{X}_j} \beta\left(\vec{x}_N, \vec{\hat{x}}_N\right) \bar{P}\left[\vec{x}_N \longrightarrow \vec{\hat{x}}_N\right] \\ &\leq \sum_{N=N_{min}}^{\infty} \sum_{\vec{x}_N} P(\vec{x}_N) \\ &\quad \times \sum_{\vec{\hat{x}}_N\neq\vec{x}_N} \beta\left(\vec{x}_N, \vec{\hat{x}}_N\right) \bar{P}\left[\vec{x}_N \longrightarrow \vec{\hat{x}}_N\right] \end{aligned}$$

which reduces to the standard expression in [16]–[18].

with $\beta\left(\vec{x}_N, \hat{\vec{x}}_N\right)$ the bit errors associated with the error event $\vec{x}_N \longrightarrow \hat{\vec{x}}_N$ and $N_{\min}$ the constraint length of the code. Hence, the average BER due to path error is given by

$$\bar{P}_b\left(\vec{s}(i) \longrightarrow \vec{s}(j)\right) \leq \frac{\mathcal{E}[n_b]}{\bar{n}}$$

where $\bar{n}$ is the average number of information bits transmitted per trellis transition.

1) Evaluation of $P\left(\vec{x}_N \longrightarrow \hat{\vec{x}}_N, \vec{m}_N|r\right)$: To evaluate $P\left(\vec{x}_N \longrightarrow \hat{\vec{x}}_N, \vec{m}_N|r\right)$, we have to find $P\left(\vec{x}_N \longrightarrow \hat{\vec{x}}_N|r, \vec{z}_{tx}[N], \vec{z}_{rx}[N]\right)$ as follows where $\vec{z}_{tx}[N]$ and $\vec{z}_{rx}[N]$ are sequences of estimated channel states at the transmitter and the receiver. The path metric of the encoded sequence, $\vec{x}_N$, at burst position r, $PM(r, \vec{x}_N)$, is given by

$$PM(r, \vec{x}_N) = \sum_{k=1}^{N} \mu_k(r) = \sum_{k=1}^{N} \left| y_k - \sqrt{\frac{E_s}{\eta_0}} z_{rx}[r,k] x_k \right|^2.$$

The error encoded sequence $\hat{\vec{x}}_N$ will be chosen if $\Delta PM(r) = PM\left(r, \hat{\vec{x}}_N\right) - PM(r, \vec{x}_N) < 0$. Note that $\Delta PM(r)$ is a Gaussian random variable with mean $\mu_{\Delta PM}(r)$ given by

$$\mu_{\Delta PM}(r) = \sum_{k=1}^{N} \sqrt{\frac{E_s}{\eta_0}} |z_{rx}[r,k]|^2 |x_k - \hat{x}_k|^2$$

and variance $\sigma^2_{\Delta PM}(r)$ bounded by

$$\sigma^2_{\Delta PM}(r) \leq 2\left(\sum_{k=1}^{N} |z_{rx}[r,k]|^2 |x_k - \hat{x}_k|^2\right) \times \left[1 + \frac{E_s}{\eta_0}|b|^2\left(\sigma_1^2[r] + \sigma_2^2[r]\right)\right].$$

Hence,

$$\begin{aligned} &P\left(\vec{x}_N \longrightarrow \hat{\vec{x}}_N|r, \vec{z}_{tx}[N], \vec{z}_{rx}[N]\right) \\ &\quad = Pr\left[\Delta PM < 0|r, \vec{z}_{tx}[N], \vec{z}_{rx}[N]\right] \\ &\quad \leq Q\left(\sqrt{\frac{E_s}{2\eta_0(1+\delta_r)} \sum_{k=1}^{N} R_{m_k} |z_{rx}[r,k]|^2 |x_k - \hat{x}_k|^2}\right) \\ &\quad \leq \frac{1}{2}\prod_{k=1}^{N} \exp\left\{-\left[\frac{R_{m_k} E_s}{4\eta_0} \frac{|z_{rx}[r,k]|^2 |x_k - \hat{x}_k|^2}{1+\delta_r}\right]\right\} \end{aligned} \quad (18)$$

where $\delta_r = E_s/\eta_0 |b|^2 (\sigma_1^2[r] + \sigma_2^2[r])$ and R_{m_k} is the number of repetitions used at the transmission mode m_k.

Unconditioning $P\left(\vec{x}_N \longrightarrow \hat{\vec{x}}_N|r, \vec{z}_{tx}[N], \vec{z}_{rx}[N]\right)$ w.r.t. $\vec{z}_{tx}[N]$ and $\vec{z}_{rx}[N]$, we obtain

$$\begin{aligned} &P\left(\vec{x}_N \longrightarrow \hat{\vec{x}}_N, \vec{m}_N|r\right) \\ &= \frac{1}{2}\prod_{k=1}^{N} \int_{\sqrt{\zeta_{m_k}/(E_s/\eta_0)}}^{\sqrt{\zeta_{m_k+1}/(E_s/\eta_0)}} \\ &\quad \times \int_0^{\infty} \exp\left\{-\left[\frac{E_s R_{m_k}}{4\eta_0} \frac{|z_{rx}[r,k]|^2 |x_k - \hat{x}_k|^2}{1+\delta_r}\right]\right\} \\ &\quad \times f(|z_{rx}[r,k]| \mid |z_{tx}[r,k]|) \\ &\quad \times d|z_{rx}[r,k]| f(|z_{tx}[r,k]|) d|z_{tx}[r,k]| \end{aligned} \quad (19)$$

where $f(|z_{rx}[r,k]| \mid |z_{tx}[r,k]|)$ is the conditional density of $|z_{rx}[r,k]|$ given $|z_{tx}[r,k]|$, and $f(|z_{tx}[r,k]|)$ is the density function of $|z_{tx}[r,k]|$.[11]

2) Joint Density of $|z_{rx}[r,k]|$ and $|z_{tx}[r,k]|$: From (2), we have

$$z_{rx}[r,k] = c[r,k] + \epsilon_1[r,k] + \epsilon_2[r,k] \quad (20)$$

and

$$\begin{aligned} &z_{tx}[r,k] \\ &\approx \begin{cases} z_{tx}[0,k] = c[0,k] + \epsilon_3[0,k] + \epsilon_4[0,k] & r \in [0, \Delta) \\ z_r x[0,k] = c[0,k] + \epsilon_1[0,k] + \epsilon_2[0,k] & r \in [\Delta, N_p) \end{cases} \end{aligned} \quad (21)$$

where $\epsilon_1[r,k]$, $\epsilon_2[r,k]$, $\epsilon_3[r,k]$, and $\epsilon_4[r,k]$ are uncorrelated Gaussian noise. Hence, $z_{rx}[r,k]$ and $z_{tx}[r,k]$ are two correlated complex Gaussian random variables. The density of the envelope $f(|z_{tx}[r,k]|)$ is well known to be Rayleigh distributed, given by

$$f(|z_{tx}[r,k]|) = \frac{|z_{tx}[r,k]|}{\sigma_b^2(r)} \exp\left\{-\frac{|z_{tx}[r,k]|^2}{2\sigma_b^2(r)}\right\}. \quad (22)$$

Similarly, the conditional density of the two envelopes is given by [19]

$$\begin{aligned} f(|z_{rx}[r,k]| \mid |z_{tx}[r,k]|) &= \frac{|z_{rx}[r,k]|}{\sigma_a^2(r)[1-\rho^2(r)]} \\ &\quad \times \exp - \left[\frac{\sigma_b^2(r)|z_{rx}[r,k]|^2 + \sigma_a^2(r)\rho^2(r)|z_{tx}[r,k]|^2}{2\sigma_a^2(r)\sigma_b^2(r)[1-\rho^2(r)]}\right] \\ &\quad \times I_0\left[\frac{|z_{rx}[r,k]||z_{tx}[r,k]|\rho(r)}{\sigma_a(r)\sigma_b(r)[1-\rho^2(r)]}\right] \end{aligned} \quad (23)$$

where

$$\sigma_a^2(r) = \frac{1}{2}\left(1 + \sigma_1^2[r] + \sigma_2^2[r]\right), \quad (24)$$

[11]Due to ideal interleaving, $f(|\vec{z}_{rx}[N]| \mid |\vec{z}_{tx}[N])$ and $f(|\vec{z}_{tx}[N])$ can be expressed as product forms.

$$\vec{P}\left(\vec{x}_n \longrightarrow \hat{\vec{x}}_N, \vec{m}_N\right) \leq \frac{1}{N_p - 1} \sum_{r=1}^{N_p-1} \prod_{k=1}^{N} \left\{ \frac{1}{R_{m_k} F(r,k)} \left[\exp\left\{-\frac{\zeta_{m_k}}{2\frac{E_s}{\eta_0}\sigma_b^2}\left(\frac{F(r,k)}{G(r,k)}\right)\right\} - \exp\left\{-\frac{\zeta_{m_k}+1}{2\frac{E_s}{\eta_0}\sigma_b^2}\left(\frac{F(r,k)}{G(r,k)}\right)\right\}\right] \right\} \quad (27)$$

$$\sigma_b^2(r) = \begin{cases} \frac{1}{2}\left(1+\sigma_3^2[r]+\sigma_4^2[r]\right), & 0 \le r < \Delta \\ \frac{1}{2}\left(1+\sigma_1^2[r]+\sigma_2^2[r]\right), & \Delta \le r \le N_p - 1 \end{cases} \tag{25}$$

and

$$\rho(r) = \frac{J_0\left(\frac{2\pi f_d T_s r}{N_u}\right)}{2\sqrt{\sigma_a^2\sigma_b^2}}. \tag{26}$$

3) Overall Expression: After integrating (19) and substituting into (17), we obtain (27), shown at the bottom of the previous page, where

$$F(r,k) = \left(1+\sigma_a^2\frac{R_{m_k}E_s}{2\eta_0}\frac{|x_k-\hat{x}_k|^2}{1+\delta_r}\right)$$

and

$$G(r,k) = 1+\sigma_a^2\left(1-\rho^2(r)\right)\frac{R_{m_k}E_s}{2\eta_0}\frac{|x_k-\hat{x}_k|^2}{1+\delta_r}.$$

APPENDIX B
DERIVATION OF $\bar{n}$

The average number of bits transmitted per trellis transition, $\bar{n}$, is equal to the ratio between the total number of bits transmitted and the total number of branch transitions passed. This is given by

$$\begin{aligned}\bar{n} =& \frac{1}{N_p-1}\sum_{r=1}^{N_p-1}\left[\int_0^{\sqrt{\zeta_2/(E_s/\eta_0)}} f\left(|z_{tx}[r]|\right)d|z_{tx}[r]| \right.\\ &\left. +\cdots+5\int_{\sqrt{\zeta_6/(E_s/\eta_0)}}^{\infty} f\left(|z_{tx}[r]|\right)d|z_{tx}[r]|\right]\\ =& \frac{1}{N_p-1}\sum_{r=1}^{N_p-1}\left[1+\frac{1}{6}\exp\left\{-\frac{\zeta_2}{2\sigma_b^2(r)\frac{E_s}{\eta_0}}\right\}\right.\\ &+\frac{1}{2}\exp\left\{-\frac{\zeta_3}{2\sigma_b^2(r)\frac{E_s}{\eta_0}}\right\}\\ &+\exp\left\{-\frac{\zeta_4}{2\sigma_b^2(r)\frac{E_s}{\eta_0}}\right\}\\ &\left.+\cdots+\exp\left\{-\frac{\zeta_6}{2\sigma_b^2(r)\frac{E_s}{\eta_0}}\right\}\right].\end{aligned} \tag{28}$$

REFERENCES

[1] S. G. Wilson, *Digital Modulation and Coding*, 1st ed. Englewood Cliffs, NJ: Prentice-Hall, 1996.

[2] J. K. Cavers, "Variable rate transmission for Rayleigh fading channel," *IEEE Trans. Commun.*, vol. COM-20, pp. 15–21, Feb. 1972.

[3] K. N. Lau, "Channel capacity and error exponent of variable rate adaptive channel coding for Rayleigh fading channels," *IEEE Trans. Commun.*, vol. 47, Sept. 1999.

[4] S. Alamouti and S. Kallel, "Adaptive trellis-coded multiple-phase-shift keying for Rayleigh fading channels," *IEEE Trans. Commun.*, vol. 42, pp. 2305–2314, June 1994.

[5] T. Ue, S. Sampei, and N. Morinaga, "Symbol rate and modulation level controlled adaptive modulation/TDMA/TDD for personal communication systems," in *Proc. IEEE VTC'95*, July 1995, pp. 306–310.

[6] Alouini and Goldsmith, "Adaptive modulation for Nakagami fading channels," in *Proc. IEEE Mini-Conf. Globecom 97*, 1997, pp. 218–223.

[7] A. J. Goldsmith and S. G. Chua, "Adaptive coded modulation," *IEEE Trans. Commun.*, vol. 46, pp. 592–602, May 1998.

[8] D. Goeckel, "Adaptive coding for fading channels using outdated channel estimates," in *Proc. IEEE VTC'98*, May 1998, pp. 1925–1929.

[9] X. Tang, M. S. Alouini, and A. Goldsmith, "The effect of channel estimation error on MQAM BER performance in Rayleigh fading channels," in *Proc. IEEE VTC'99*, May 1999, pp. 1111–1115.

[10] J. K. Cavers, "An analysis of pilot symbol assisted modulation for Rayleigh fading channels," *IEEE Trans. Veh. Technol.*, vol. 40, pp. 686–693, Nov. 1991.

[11] A. J. Viterbi, J. K. Wolf, E. Zehavi, and R. Padovani, "A pragmatic approach to trellis-coded modulation," *IEEE Commun. Mag.*, pp. 11–19, July 1989.

[12] K. N. Lau, "Variable Rate Adaptive Channel Coding for Mobile Cellular Systems," Ph.D., Dept. Eng., Univ. of Cambridge, Cambridge, U.K., 1997.

[13] C. W. Therrien, *Discrete Random Signals and Statistical Signal Processing*, 1st ed. Englewood Cliffs, NJ: Prentice-Hall, 1992.

[14] J. G. Proakis, *Digital Communications*, 3rd ed, NY: McGraw-Hill, 1995.

[15] G. Ungerboeck, "Channel coding with multilevel/phase signals," *IEEE Trans. Inform. Theory*, vol. IT-28, pp. 55–67, Jan. 1982.

[16] C. Schlegel and D. J. Costello, "Bandwidth efficient coding for fading channels: Code construction and performance analysis," *IEEE Trans. Commun.*, vol. 37, pp. 1356–1368, Dec. 1989.

[17] D. Divsalar and M. K. Simon, "The design of trellis coded MPSK for fading channels: Performance criteria," *IEEE Trans. Communs.*, vol. 36, pp. 1004–1011, Sept. 1988.

[18] ——, "Trellis coded modulation for 4800–9600 bits/s transmission over a fading mobile satellite channel," *IEEE J. Select. Areas Commun.*, vol. SAC-5, pp. 162–175, Feb. 1987.

[19] A. Papoulis, *Probability, Random Variables, and Stochastic Processes*, 3rd ed, Singapore: McGraw-Hill, 1991.

Vincent K. N. Lau received the B.Eng. degree (1st Hons with Distinction) from the University of Hong Kong in 1992 and the Ph.D. degree in mobile communications from the University of Cambridge, Cambridge, U.K., in 1997. His dissertation was on the practical design and information theoretical aspects of variable rate adaptive channel coding for wireless communications.

He joined Hong Kong Telecom in 1992 for three years as a Project Engineer and was later promoted to System Engineer, responsible for transmissions equipment. He obtained the Sir Edward Youde Memorial Fellowship and the Croucher Foundation in 1995 and went to the University of Cambridge. In 1997, he joined Lucent Technologies—Bell Labs as a Member of Ttechnical Staff. He was engaged in the design and development of third-generation wide-band CDMA. His research interest includes information theory, adaptive channel coding and modulation, digital transceiver design, power control, and CREST factor control algorithms, QoS-based multiple access protocols in 3G wideband CDMA systems, as well as short-range wireless *ad hoc* networking design. He joined the Department of Electrical and Electronic Engineering, Hong Kong University, in 1999. He was appointed the Co-director of the Information Engineering Programme and the Co-director of the 3G Ttechnology Center at the University of Hong Kong. He was also the cofounder of DAX Group Ltd., a technology startup. He has published more than 40 papers and has two U.S. patents pending. He has returned to the Wireless Advanced Technology Lab of Lucent Technologies.

Malcolm D. Macleod (M'84) was born in 1953 in Cathcart, Glasgow, U.K. He received the B.A. (with distinction), M.A., and Ph.D. degrees from the University of Cambridge, Cambridge, U.K., in 1974, 1978, and 1979, respectively. His dissertation was on discrete optimization of DSP systems.

From 1978 to 1988, he worked for Cambridge Consultants, Ltd., on a wide range of signal processing, electronics, and software research and development projects. From 1988 to 1995, he was a Lecturer with the Signal Processing and Communications Group, Engineering Department, Cambridge University. In 1995, he was appointed the Director of Research in the Department. His main research interests are in high-resolution spectrum estimation and beam forming, digital filter design, nonlinear filtering, adaptive filtering, optimal detection, advanced modulation methods, and applications in sonar, instrumentation, and communication systems